^{133}In: A Rosetta Stone for Decays of r-Process Nuclei

Z. Y. Xu[1], M. Madurga,[1] R. Grzywacz,[1,2] T. T. King,[1,2] A. Algora,[3,4] A. N. Andreyev,[5,6] J. Benito,[7,8,9] T. Berry,[10]
M. J. G. Borge,[11] C. Costache,[12] H. De Witte,[13] A. Fijalkowska,[14,15] L. M. Fraile,[7] H. O. U. Fynbo,[16] A. Gottardo,[17]
C. Halverson,[1] L. J. Harkness-Brennan,[18] J. Heideman,[1] M. Huyse,[13] A. Illana,[13,19] Ł. Janiak,[15,20] D. S. Judson,[18]
A. Korgul,[15] T. Kurtukian-Nieto,[21] I. Lazarus,[22] R. Lică,[23,12] R. Lozeva,[24] N. Marginean,[12] R. Marginean,[12] C. Mazzocchi,[15]
C. Mihai,[12] R. E. Mihai,[12] A. I. Morales,[3] R. D. Page,[18] J. Pakarinen,[19,25] M. Piersa-Siłkowska,[15,23] Zs. Podolyák,[10]
P. Sarriguren,[11] M. Singh,[1] Ch. Sotty,[12] M. Stepaniuk,[15] O. Tengblad,[11] A. Turturica,[12] P. Van Duppen,[13] V. Vedia,[7]
S. Viñals,[11] N. Warr,[26] R. Yokoyama,[1] and C. X. Yuan[27]

[1]*Department of Physics and Astronomy, University of Tennessee, Knoxville, Tennessee 37996, USA*
[2]*Physics Division, Oak Ridge National Laboratory, Oak Ridge, Tennessee 37831, USA*
[3]*Instituto de Física Corpuscular, CSIC-Universidad de Valencia, E-46071 Valencia, Spain*
[4]*Institute of Nuclear Research (ATOMKI), P. O. Box 51, H-4001 Debrecen, Hungary*
[5]*School of Physics, Engineering and Technology, University of York, North Yorkshire YO10 5DD, United Kingdom*
[6]*Advanced Science Research Center, Japan Atomic Energy Agency, Tokai, Ibaraki 319-1195, Japan*
[7]*Grupo de Física Nuclear and IPARCOS, Facultad de CC. Físicas, Universidad Complutense de Madrid,
E-28040 Madrid, Spain*
[8]*Istituto Nazionale di Fisica Nucleare, Sezione di Padova, I-35131, Padova, Italy*
[9]*Dipartimento di Fisica e Astronomia, Università di Padova, I-35131 Padova, Italy*
[10]*Department of Physics, University of Surrey, Guildford GU2 7XH, United Kingdom*
[11]*Instituto de Estructura de la Materia, IEM-CSIC, Serrano 113 bis, E-28006 Madrid, Spain*
[12]*Horia Hulubei National Institute for Physics and Nuclear Engineering, RO-077125 Bucharest, Romania*
[13]*KU Leuven, Instituut voor Kern- en Stralingsfysica, B-3001 Leuven, Belgium*
[14]*Department of Physics and Astronomy, Rutgers University, New Brunswick, New Jersey 08903, USA*
[15]*Faculty of Physics, University of Warsaw, PL 02-093 Warsaw, Poland*
[16]*Department of Physics and Astronomy, Aarhus University, DK-8000 Aarhus C, Denmark*
[17]*IPN, IN2P3-CNRS, Université Paris-Sud, Université Paris Saclay, 91406 Orsay Cedex, France*
[18]*Department of Physics, Oliver Lodge Laboratory, University of Liverpool, Liverpool L69 7ZE, United Kingdom*
[19]*University of Jyväskylä, Department of Physics, P.O. Box 35, FI-40014 Jyväskylä, Finland*
[20]*National Centre for Nuclear Research, 05-400 Otwock, świerk, Poland*
[21]*CENBG, Université de Bordeaux—UMR 5797 CNRS/IN2P3, Chemin du Solarium, 33175 Gradignan, France*
[22]*STFC Daresbury, Daresbury, Warrington WA4 4AD, United Kingdom*
[23]*ISOLDE, EP Department, CERN, CH-1211 Geneva, Switzerland*
[24]*Université Paris-Saclay, IJCLab, CNRS/IN2P3, F-91405 Orsay, France*
[25]*Helsinki Institute of Physics, University of Helsinki, P.O. Box 64, FIN-00014 Helsinki, Finland*
[26]*Institut für Kernphysik, Universität zu Köln, 50937 Köln, Germany*
[27]*Sino-French Institute of Nuclear Engineering and Technology, Sun Yat-Sen University,
Zhuhai, 519082, Guangdong, China*

The β decays from both the ground state and a long-lived isomer of ^{133}In were studied at the ISOLDE Decay Station (IDS). With a hybrid detection system sensitive to β, γ, and neutron spectroscopy, the comparative partial half-lives ($\log ft$) have been measured for all their dominant β-decay channels for the first time, including a low-energy Gamow-Teller transition and several first-forbidden (FF) transitions. Uniquely for such a heavy neutron-rich nucleus, their β decays selectively populate only a few isolated neutron unbound states in ^{133}Sn. Precise energy and branching-ratio measurements of those resonances allow us to benchmark β-decay theories at an unprecedented level in this region of the nuclear chart. The results show good agreement with the newly developed large-scale shell model (LSSM) calculations. The experimental findings establish an archetype for the β decay of neutron-rich nuclei southeast of ^{132}Sn and

will serve as a guide for future theoretical development aiming to describe accurately the key β decays in the rapid-neutron capture (r-) process.

Introduction.—The rapid-neutron capture (r) process is responsible for the creation of half of the heavy elements in the universe [1,2]. Many stable nuclei present today are decay products of the very short-lived nuclei produced in extreme environments such as neutron star mergers or supernovae [3,4]. Most of these progenitor nuclei have large neutron-to-proton ratios, and state-of-the-art nuclear research facilities cannot produce samples in sufficient quantities for experimental work. Yet, measured elemental abundance in stars cannot be explained without knowing their decay properties including half-lives $T_{1/2}$ and β-delayed neutron-emission probabilities P_n [5–7]. Modern nuclear theories were developed to predict these quantities for radioactive isotopes far from their stable counterparts [8–12]. To verify those models, experimental efforts were carried out continuously pursuing those gross decay properties of isotopes close to the r-process path [13–19]. Because of the complicated nature of those decays far off stability, the agreement with model predictions can be ambiguous, i.e., theories may arrive at a similar gross property for a single isotope using different footing. In addition, it is generally hard to find conclusive answers on how to improve the theories when a discrepancy emerges. Thus, it is desirable to measure the observables capable of benchmarking β-decay calculations on a more fundamental level. In this Letter, we report a β-decay strength measurement of ^{133}In ($Z = 49$, $N = 84$), a nucleus close to many r-process nuclei southeast of ^{132}Sn ($Z = 50$, $N = 82$), see Fig. 1. We examined decays from both the ground state (^{133g}In) and the isomer (^{133m}In) via β-delayed γ and neutron spectroscopy, demonstrating as a textbook example the interplay between allowed Gamow-Teller (GT) and first-forbidden (FF) transitions in extremely neutron-rich nuclei near the r-process path. Thus, our measurement must be accounted for by the models used to predict the decay properties of the r-process nuclei.

In the nuclear shell model [21,22], the doubly magic ^{132}Sn arranges protons (π) and neutrons (ν), respectively, into the closed $3\hbar\omega$ and $4\hbar\omega$ major shells, see Fig. 1. To the southeast of ^{132}Sn, where ^{133}In resides, the proton Fermi surface is near the $\pi g_{9/2}$ orbital ($3\hbar\omega$) whereas neutrons start filling the $5\hbar\omega$ shell above $N = 82$, generating large $2\hbar\omega$ asymmetry between the proton and neutron Fermi surfaces. Since $\pi g_{9/2}$ is partially occupied, the GT transformation $\nu g_{7/2} \rightarrow \pi g_{9/2}$ (the red arrow in Fig. 1) is expected to be strong. Other competing GT channels have to induce proton excitation across the $Z = 50$ shell (e.g., $\nu g_{7/2} \rightarrow \pi g_{7/2}$) and thus are much less favorable energetically. Consequently, the $\nu g_{7/2} \rightarrow \pi g_{9/2}$ transformation is

the single dominant decay channel in the majority of nuclei in this region. Besides, a few FF transitions contribute significantly to the β-decay rates by involving neutron and proton orbitals with opposite parities near the Fermi surface (the gray arrows in Fig. 1, e.g., $\nu h_{11/2} \rightarrow \pi g_{9/2}$). The proximity of ^{133}In to the ^{132}Sn core reduces the number of active nucleons and the degrees of freedom in the decay process, making it an ideal ground to validate nuclear theories. On the other hand, the extreme neutron excess ($N - Z = 35$) and large Q_β energy window (> 13 MeV) give ^{133}In more complete access than nearby nuclei, such as ^{131}In ($Z = 49$, $N = 82$) and ^{133}Sn ($Z = 50$, $N = 83$), to the dominant β-decay channels that are responsible for the gross decay properties in the region. Overall, the unique combination of a large variety of decay modes and simple representation makes ^{133}In a perfect study-case nucleus, or
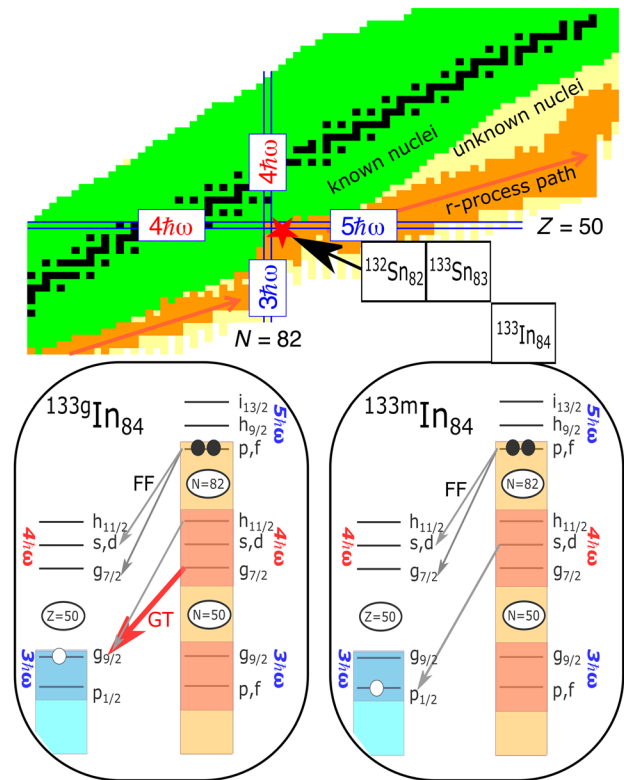

FIG. 1. Top: chart of nuclei centered on ^{133}In (red star). The label $\hbar\omega$ refers to the harmonic-oscillator shells around ^{132}Sn. The r-process path is taken from Ref. [20]. Bottom: proton and neutron single-particle ($s.p.$) diagram with dominant β-decay channels in ^{133g}In and ^{133m}In. Red and gray arrows represent GT and FF transitions, respectively.

a Rosetta stone, to understand how the *r*-process nuclei decay near the neutron $N = 82$ shell closure.

We studied the β decay of ^{133}In using the neutron time-of-flight (TOF) technique in combination with a high-resolution γ-ray spectroscopic system. The β decay mostly populated neutron-unbound states in ^{133}Sn, which promptly decayed to ^{132}Sn via neutron emission [23–25]. If the neutron emission feeds an excited state in ^{132}Sn, the nucleus will also undergo γ decay(s) to the ground state. Although several groups have conducted spectroscopic studies of ^{133}Sn in the past [23,24,26–28], the knowledge of states above the neutron separation energy was scarce due to either the weak production rate or inefficient neutron detection. By taking advantage of neutron and γ spectroscopy measured in coincidence with β decay, we revealed for the first time all the dominant β-decay transitions in ^{133}In above the neutron separation energy. Owing to selective laser ionization of the ^{133}In samples [24], the decays from the $9/2^+$ ground state (^{133g}In) and the $1/2^-$ isomer (^{133m}In) were separated unambiguously. The simple structure of ^{133}Sn, the β-decay selection rules, and the laser ionization all together allowed us to achieve a superior precision measurement. In addition, we used the new observation to benchmark large-scale shell-model (LSSM) calculations. The new measurement provides valuable insights into understanding the β decays of *r*-process nuclei.

Experiment and result.—The Isotope Separator On-Line (ISOLDE) facility at CERN [29] and resonance ionization laser ion source [30] produced the isotopes of interest. Through the general purpose separator (GPS) [29], the beams were brought to the ISOLDE Decay Station for β-decay measurements. The neutron TOF spectra measured in coincidence with the β decay of ^{133}In are presented in Fig. 2, with Fig. 2(a) corresponding to the pure ground-state decay and Fig. 2(b) to an admixture of ground-state (40%) and isomeric decays (60%). Those neutrons were emitted from the neutron-unbound states in ^{133}Sn after being populated in the β decay. Neutron emissions may leave the residual ^{132}Sn nucleus in an excited state. However, we did not observe any of the strong neutron peaks in Fig. 2 coinciding with the ^{132}Sn γ decay, see Fig. 2(c), implying strong direct ground-state feedings in the neutron emissions. The spectra are fitted by a neutron response function (magenta) consisting of 19 and 13 peaks in ^{133g}In (blue) and ^{133m}In (red) decays, respectively. We extracted the excitation energies ($E_{\rm ex}$) and decay probabilities (I_β) of individual states from the fitting result. The full details of the experimental setup, data analysis, and the list of neutron unbound states identified in ^{133}Sn are presented in Ref. [31].

The main achievement of this Letter is the observation and quantification of the β-decay channels in ^{133g,m}In. The strongest transitions are mediated by transforming a
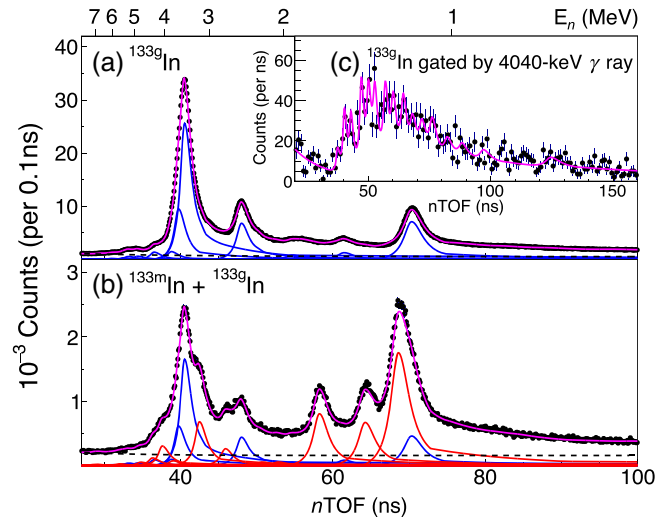

FIG. 2. Neutron TOF spectra taken in coincidence with the ^{133}In β decays, with (a) corresponding to the pure ground-state decay and (b) to an admixture of ground-state (40%) and isomeric decays (60%). The inset (c) shows the ground-state spectrum in coincidence with the 4041-keV γ decay in ^{132}Sn. On top of the background (dashed line), the spectra are fitted by the neutron response functions (magenta) consisting of 19 (blue) and 13 (red) peaks in the ground-state and isomeric decays, respectively.

neutron from inside the $N = 82$ core to a proton on either $\pi g_{9/2}$ (ground-state decay) or $\pi p_{1/2}$ (isomeric decay), leaving the proton $Z = 50$ shell closed and two neutrons outside $N = 82$ coupled to a spin-zero pair, see Fig. 1. We refer to the ^{133}Sn states so populated as $\nu 2p\text{-}1h$ (neutron two particle one hole) states hereafter. Using the analysis methodology detailed in Ref. [31], we identified four such states, including the $11/2^-(\nu h_{11/2}^{-1})$ state at 3.564(1) MeV [24], the $3/2^+(\nu d_{3/2}^{-1})$ state at 3.62(2) MeV, the $1/2^+(\nu s_{1/2}^{-1})$ state at 3.79(2) MeV, and the $7/2^+(\nu g_{7/2}^{-1})$ state at 5.93(9) MeV (the superscript of an orbital indicates occupation number, being positive for particles and negative for holes). Our experiment observed most of these states for the first time, the sole exception being the $11/2^-$ state [23,24,28]. We extracted comparative partial half-lives ($\log ft$) for those transitions. The $\log ft$ values quantify the strength of a given β-decay transition and correlate to the β-decay strength as $S_\beta = 1/ft$ [32], where f is the Fermi function [33] for the electron distribution feeding a given state and $t = T_{1/2}/I_\beta$ is the partial half-life of a transition with I_β probability. From the $9/2^+$ ground state, the $\log ft$ values to the $11/2^-$ and $7/2^+$ states are 5.7(1) and 4.7(1), respectively. From the $1/2^-$ isomer, the $\log ft$ values to the $3/2^+$ and $1/2^+$ states are 5.4(1) and 5.8(1), respectively. Based on the constraints imposed by β-decay selection rules, the $7/2^+$ state was populated via a GT transition, whereas the other three states were fed by FF transitions. These assignments are in line with the systematics gleaned from the $\log ft$ values mentioned above [34].

Comparison with LSSM.—We carried out LSSM calculations to interpret our results quantitatively. A model space containing multiple complete proton and neutron major shells around ^{132}Sn exceeds current computational capability. To focus on the strong decay channels in ^{133}In, e.g., $\nu g_{7/2} \rightarrow \pi g_{9/2}$, we built the model space on a ^{88}Sr core ($Z = 38$, $N = 50$), including the $0g_{7/2}$, $1d_{5/2}$, $1d_{3/2}$, $2s_{1/2}$, $0h_{11/2}$, $1f_{7/2}$ orbitals for valence neutrons and the $1p_{1/2}$, $0g_{9/2}$, $0g_{7/2}$, $1d_{5/2}$, $1d_{3/2}$, $2s_{1/2}$ orbitals for valence protons. This choice retains important orbital partners relevant for β decay, see Fig. 1. We truncated the number of allowed p-h excitations across ^{132}Sn to $2p$-$2h$ as the first-order approximation. We used three sets of two-body interactions constructed from the effective nucleon-nucleon (NN) potentials of (i) N^{3}LO [35], (ii) Argonne V18 [36], and (iii) V$_{MU}$ plus M3Y [37,38]. N^{3}LO and V18 were derived using the many-body perturbation theory [39], with the procedure outlined in Ref. [40]. V$_{MU}$ was obtained by computing the matrix elements directly within our model space. We determined the single-particle ($s.p.$) energies from the spectroscopic data in the vicinity of ^{132}Sn. The GT and FF operators were defined in Ref. [41], and their effective scaling factors were listed as follows that best reproduce our data:

$$q(\text{GT}) = 0.6, \qquad q(M_0^T) = 1.5, \qquad q(M_0^S) = 0.6,$$
$$q(x) = 0.5, \qquad q(u) = 0.4, \qquad q(z) = 0.8.$$

We first examined the individual transitions populating the four $\nu 2p$-$1h$ states, see Figs. 3(a)–3(d). All three nuclear potentials reproduced the experimental FF strengths feeding the $11/2^-$, $3/2^+$, and $1/2^+$ states at lower

excitation energy. Additionally, they gave consistent microscopic compositions of those states: the greatest fractions in the $11/2^-$ and $3/2^+$ wave functions were $\nu h_{11/2}^{-1} \times f_{7/2}^2$ and $\nu d_{3/2}^{-1} \times f_{7/2}^2$, respectively ($> 85\%$). The $1/2^+$ state was somewhat mixed, with the leading order term $\nu s_{1/2}^{-1} \times f_{7/2}^2$ being less than 55%. Regarding the $7/2^+$ state, the calculations diverged in the GT strength, giving 36×10^{-6} s^{-1} (V$_{MU}$), 37×10^{-6} s^{-1} (V18), and 19×10^{-6} s^{-1} (N^{3}LO) respectively. Although all models predicted a similar fraction of $\nu g_{7/2}^{-1} \times f_{7/2}^2$ ($\sim 45\%$) in their wave functions, they differed in the amounts of proton excitation across $Z = 50$, 0.4 in N^{3}LO, and 0.1 in V18 and V$_{MU}$. The experimental GT strength, $20(4) \times 10^{-6}$ s^{-1}, was as quenched as the N^{3}LO prediction, suggesting sizeable proton core excitation contributing to the state. The comparison reveals the sensitivity of this particular GT decay strength to the employed NN interactions. Considering this $\nu g_{7/2} \rightarrow \pi g_{9/2}$ transition dominates the decay rate (and half-life) in not only ^{133}In but also a large number of neutron-rich nuclei southeast of ^{132}Sn, it is of paramount importance to reproduce this decay in ^{133}In in any theoretical calculations aiming to provide reliable nuclear-decay input to astrophysical applications.

Next, we presented in Figs. 3(e) and 3(f) the cumulative β-strength distribution from the experiment and LSSM with N^{3}LO. The calculations nicely follow the experimental distribution of both states below 9 MeV, with the deviation less than 2-σ uncertainty. The resultant half-lives are 145 and 169 ms for the ground state and isomer, respectively, being consistent with the literature values (162 and 167 ms) [24]. Towards higher excitation energy, a sharp kink emerged in the calculations and drove the distributions up over the
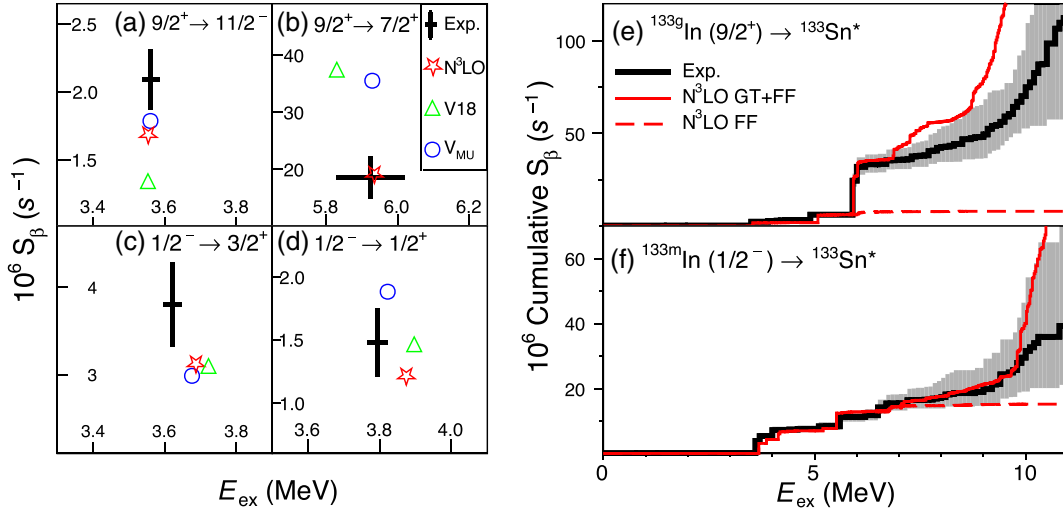

FIG. 3. Comparisons of excitation energy and decay strength between LSSM and experimental data. Figures (a)–(d) show the results of four individual transitions populating the $\nu 2p$-$1h$ states. Figures (e) and (f) present cumulative strength distribution up to $E_{ex} = 11$ MeV for ^{133g,m}In, respectively. The calculation only includes the results from N^{3}LO because of its better agreement in the GT strength. The theoretical FF contribution is drawn explicitly in dashed lines.

experimental ones. Because FF decays are extremely weak there, see Figs. 3(e) and 3(f), those strengths are ascribed to the GT decays involving both the neutron and proton orbitals in the 50–82 shell, or the $4\hbar\omega$ shell, in Fig. 1. The disagreement is most likely caused by the truncation of $2p$-$2h$ excitation across ^{132}Sn, which is not sufficient to describe fully the NN correlations and strength distribution at such high energy. Even though it has a relatively minor impact on the calculated half-lives and thus the r process, the problem will have to be addressed with more advanced theoretical treatment in the future.

Feedback to global calculations.—Although the LSSM calculations achieved a satisfactory agreement with our data, it is impractical to make systematic calculations across the nuclear chart due to the large model spaces. Therefore, global nuclear models are indispensable for modeling the r process. Our new measurements can serve as constraints and validation points to improve the accuracy of those global models beyond what was previously achievable. The measured branching ratios from this Letter allowed the extraction of partial half-lives of GT and FF transitions of an r-process nucleus. According to our LSSM calculations in Fig. 3, FF transitions dominate the strength below the GT peak at 6 MeV, whereas those above 6 MeV are mostly GT transitions. Therefore, the partial half-life of FF transitions is obtained by summing β-decay probabilities below the $7/2^+$ state at 5.93 MeV, including the bound states [23–25]. The GT transitions contain the rest of the feeding intensities from 5.93 MeV onward. To accommodate the model dependency, we estimated a systematic uncertainty of attributing 50% of the strength above 6 MeV to FF transitions. The resultant partial half-lives are $t^{GT} = 260(40)$ and $t^{FF} = 435(60)$ ms for ^{133g}In, and $t^{GT} = 1130(500)$ and $t^{FF} = 195(10)$ ms for ^{133m}In. Although the two states have similar half-lives, the ground-state decay is dominated by GT transitions, whereas the isomeric decay is mostly carried by FF transitions.

Because global models only predict ground-state decays to date, the comparison in Fig. 4 is presented for ^{133g}In exclusively. The global models include Möller03 (FRDM + QRPA) [8], Borzov16 (DF + CQRPA) [42], Marketin16 (RHB + pn-RQRPA) [9], Ney20 (EFA-pnFAM) [12], and Sarriguren22 (HF + BCS + QRPA) [43]. All five are the QRPA calculations that differ in their degree of self-consistency, density functional, or calculation method. In the results of Moller03, the discrepancy is mainly driven by the GT decays, while in Marketin16, it is caused by FF transitions with overestimated strength. Although Ney20 finds a reasonable ratio between the GT and FF strengths, its absolute decay rates are underestimated by more than a factor of 2. The deviations suggest the strength distributions of those models need to be revised for ^{133}In to improve their prediction power for other r-process nuclei further away from ^{132}Sn. Borzov16 achieves the best agreement overall with the experimental data. Even though
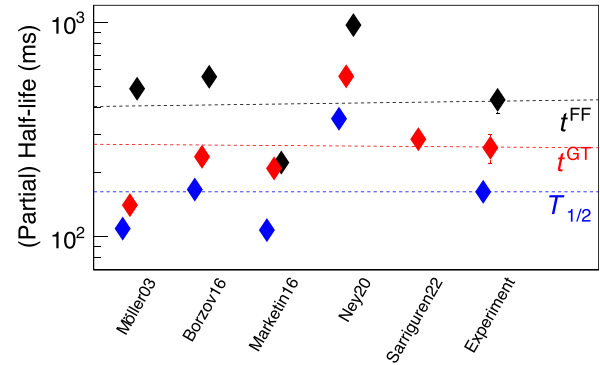

FIG. 4. Comparison between several global calculations and the experimental half-life (guided by dashed lines) of ^{133g}In. The total half-life (blue) is divided into GT (red) and FF (black) partial half-lives, with the experimental values being 260(40) and 435(60) ms, respectively. Calculations are explained in the main text.

Sarriguren22 does not include FF decays, it provides a reasonable partial GT half-life for ^{133g}In.

Summary and prospects.—In conclusion, we established with high precision the β-decay strength distribution of ^{133g,m}In. Its ground-state decay is dominated by a GT transformation, while the isomer almost exclusively decays through FF transitions. The experimental findings were used to benchmark LSSM calculations with effective interactions. For the GT transformation $9/2^+ \rightarrow 7/2^+$, only N^{3}LO produced a good agreement with the data. In contrast, all the models agreed with the FF decays at lower excitation energy. The comparison of several existing global models shows a wide range of competition between GT and FF transitions in this simple nucleus, with only Borzov16 estimating their relative contributions and absolute decay rates correctly. It is noteworthy that the novel *ab initio* theories developed rapidly in nuclear physics during the last decade. While not yet available for global predictions, they have already given essential advancement in understanding nuclear β-decay probabilities [44]. The measurements from this Letter will serve as an anchor point on the neutron-rich side of the nuclear chart, where the strengths are more fragmented and quenched than those in the ^{100}Sn region along the $Z = N$ line [45,46].

[1] E. M. Burbidge, G. R. Burbidge, W. A. Fowler, and F. Hoyle, Rev. Mod. Phys. **29**, 547 (1957).

[2] A. G. Cameron, *Stellar Evolution, Nuclear Astrophysics, and Nucleogenesis. Second Edition*, Technical Report (Atomic Energy of Canada Ltd, Chalk River, Ontario, 1957), Vol. CRL-41.

[3] E. Pian *et al.*, Nature (London) **551**, 67 (2017).

[4] D. Yong, C. Kobayashi, G. S. Da Costa, M. S. Bessell, A. Chiti, A. Frebel, K. Lind, A. D. Mackey, T. Nordlander, M. Asplund, A. R. Casey, A. F. Marino, S. J. Murphy, and B. P. Schmidt, Nature (London) **595**, 223 (2021).

[5] J. J. Cowan, C. Sneden, J. E. Lawler, A. Aprahamian, M. Wiescher, K. Langanke, G. Martínez-Pinedo, and F.-K. Thielemann, Rev. Mod. Phys. **93**, 015002 (2021).

[6] M. Mumpower, R. Surman, G. McLaughlin, and A. Aprahamian, Prog. Part. Nucl. Phys. **86**, 86 (2016).

[7] M. Arnould and S. Goriely, Prog. Part. Nucl. Phys. **112**, 103766 (2020).

[8] P. Möller, B. Pfeiffer, and K.-L. Kratz, Phys. Rev. C **67**, 055802 (2003).

[9] T. Marketin, L. Huther, and G. Martínez-Pinedo, Phys. Rev. C **93**, 025805 (2016).

[10] H. Koura, T. Yoshida, T. Tachibana, and S. Chiba, EPJ Web Conf. **146**, 12003 (2017).

[11] P. Möller, M. Mumpower, T. Kawano, and W. Myers, At. Data Nucl. Data Tables **125**, 1 (2019).

[12] E. M. Ney, J. Engel, T. Li, and N. Schunck, Phys. Rev. C **102**, 034326 (2020).

[13] S. Nishimura *et al.*, Phys. Rev. Lett. **106**, 052502 (2011).

[14] A. I. Morales *et al.*, Phys. Rev. Lett. **113**, 022702 (2014).

[15] Z. Y. Xu *et al.*, Phys. Rev. Lett. **113**, 032505 (2014).

[16] G. Lorusso *et al.*, Phys. Rev. Lett. **114**, 192501 (2015).

[17] J. Wu *et al.*, Phys. Rev. Lett. **118**, 072701 (2017).

[18] O. Hall *et al.*, Phys. Lett. B **816**, 136266 (2021).

[19] V. H. Phong *et al.*, Phys. Rev. Lett. **129**, 172701 (2022).

[20] J. Lippuner and L. F. Roberts, Astrophys. J. **815**, 82 (2015).

[21] M. G. Mayer, Phys. Rev. **75**, 1969 (1949).

[22] O. Haxel, J. H. D. Jensen, and H. E. Suess, Phys. Rev. **75**, 1766 (1949).

[23] P. Hoff *et al.* (ISOLDE Collaboration), Phys. Rev. Lett. **77**, 1020 (1996).

[24] M. Piersa *et al.* (IDS Collaboration), Phys. Rev. C **99**, 024304 (2019).

[25] J. Benito *et al.* (IDS Collaboration), Phys. Rev. C **102**, 014328 (2020).

[26] K. L. Jones *et al.*, Nature (London) **465**, 454 (2010).

[27] J. M. Allmond *et al.*, Phys. Rev. Lett. **112**, 172701 (2014).

[28] V. Vaquero *et al.*, Phys. Rev. Lett. **118**, 202502 (2017).

[29] R. Catherall, W. Andreazza, M. Breitenfeldt, A. Dorsival, G. J. Focker, T. P. Gharsa, T. J. Giles, J.-L. Grenard, F. Locci, P. Martins, S. Marzari, J. Schipper, A. Shornikov, and T. Stora, J. Phys. G **44**, 094002 (2017).

[30] V. Fedosseev, K. Chrysalidis, T. D. Goodacre, B. Marsh, S. Rothe, C. Seiffert, and K. Wendt, J. Phys. G **44**, 084006 (2017).

[31] Z. Y. Xu *et al.*, companion paper, Phys. Rev. C **108**, 014314 (2023).

[32] C. Duke, P. Hansen, O. Nielsen, and G. Rudstam, Nucl. Phys. **A151**, 609 (1970).

[33] J. Orear, *Nuclear Physics: A Course Given by Enrico Fermi at the University of Chicago. Revised edition.* (University of Chicago Press, Chicago, 1950).

[34] B. Singh, J. Rodriguez, S. Wong, and J. Tuli, Nucl. Data Sheets **84**, 487 (1998).

[35] D. R. Entem and R. Machleidt, Phys. Rev. C **68**, 041001(R) (2003).

[36] R. B. Wiringa, V. G. J. Stoks, and R. Schiavilla, Phys. Rev. C **51**, 38 (1995).

[37] T. Otsuka, T. Suzuki, M. Honma, Y. Utsuno, N. Tsunoda, K. Tsukiyama, and M. Hjorth-Jensen, Phys. Rev. Lett. **104**, 012501 (2010).

[38] G. Bertsch, J. Borysowicz, H. McManus, and W. Love, Nucl. Phys. **A284**, 399 (1977).

[39] M. Hjorth-Jensen, T. T. Kuo, and E. Osnes, Phys. Rep. **261**, 125 (1995).

[40] M. Horoi and B. A. Brown, Phys. Rev. Lett. **110**, 222502 (2013).

[41] S. Yoshida, Y. Utsuno, N. Shimizu, and T. Otsuka, Phys. Rev. C **97**, 054321 (2018).

[42] I. N. Borzov, Phys. At. Nucl. **79**, 910 (2016).

[43] P. Sarriguren, E. M. de Guerra, and A. Escuderos, Nucl. Phys. **A691**, 631 (2001); P. Sarriguren (private communication).

[44] P. Gysbers, G. Hagen, J. D. Holt, G. R. Jansen, T. D. Morris, P. Navrátil, T. Papenbrock, S. Quaglioni, A. Schwenk, S. R. Stroberg, and K. A. Wendt, Nat. Phys. **15**, 428 (2019).

[45] C. B. Hinke *et al.*, Nature (London) **486**, 341 (2012).

[46] D. Lubos *et al.*, Phys. Rev. Lett. **122**, 222502 (2019).

[47] N. Shimizu, T. Mizusaki, Y. Utsuno, and Y. Tsunoda, Comput. Phys. Commun. **244**, 372 (2019).